Biomaterials 234 (2020) 119756

Contents lists available at ScienceDirect

Biomaterials

journal homepage: www.elsevier.com/locate/biomaterials

Force-dependent extracellular matrix remodeling by early-stage cancer cells alters diffusion and induces carcinoma-associated fibroblasts

Wei-Hung Jung[a,e,f], Nicholas Yam[b,e,f], Chin-Chi Chen[c], Khalid Elawad[d], Brian Hu[a], Yun Chen[a,e,f,*]

[a] Department of Mechanical Engineering, Johns Hopkins University, Baltimore, MD, 21218, USA
[b] Department of Biomedical Engineering, Johns Hopkins University, Baltimore, MD, 21218, USA
[c] Department of Pathology, Sidney Kimmel Comprehensive Cancer Center, Johns Hopkins Medical Institutions, Baltimore, MD, 21231, USA
[d] Department of Materials Science and Engineering, Johns Hopkins University, Baltimore, MD, 21218, USA
[e] The Institute for NanoBioTechnology, Johns Hopkins University, Baltimore, MD, 21218, USA
[f] Center for Cell Dynamics, Johns Hopkins University, MD, 21205, USA

ARTICLE INFO

Keywords:
Extracellular matrix remodeling
Tumor microenvironment
Carcinoma-associated fibroblast
Early-stage cancer
Diffusion

ABSTRACT

It is known cancer cells secrete cytokines inducing normal fibroblasts (NFs) to become carcinoma-associated fibroblasts (CAFs). However, it is not clear how the CAF-promoting cytokines can effectively navigate the dense ECM, a diffusion barrier, in the tumor microenvironment to reach NFs during the early stages of cancer development. In this study, we devised a 3D coculture system to investigate the possible mechanism of CAF induction at early stages of breast cancer. We found that in a force-dependent manner, ECM fibrils are radially aligned relative to the tumor spheroid. The fibril alignment enhances the diffusion of exosomes containing CAF-promoting cytokines towards NFs. Suppression of force generation or ECM remodeling abolishes the enhancement of exosome diffusion and the subsequent CAF induction. In summary, our finding suggests that early-stage, pre-metastatic cancer cells can generate high forces to align the ECM fibrils, thereby enhancing the diffusion of CAF-promoting exosomes to reach the stroma and induce CAFs.

1. Introduction

Detection of carcinoma-associated fibroblasts (CAFs) in cancer patients is associated with poor prognosis [1–3]. The role of CAFs in tumor progression has been extensively studied [2,4–15]. For example, CAFs can mechanically and chemically remodel the tumor microenvironment to promote efficient metastasis [9,13,16,17]. CAFs also secrete cytokines to promote proliferation and to resist apoptosis in cancer cells [18,19]. Despite the extensive studies regarding how CAFs facilitate tumor progression, it is yet to be elucidated how CAFs are induced from the normal fibroblast (NFs) *in vivo*. Although direct incubation of secreted CAF-promoting factors from breast cancer cells with NFs, such as cytokines (e.g. TGF-β), microRNAs [20,21] and exosomes containing cytokine and/or microRNA [22–25], were shown to induce CAF phenotypes *in vitro*, it is not known how CAF-promoting factors reach stromal NFs *in vivo,* especially during the early stages of cancer development. CAF induction can occur at early cancer stages [26], where cancer cells are not yet invasive, secrete low matrix metalloproteinase (MMPs) [27,28] and still are restricted by the intact extracellular matrix (ECM) surrounding the tumor. For CAF-promoting factors to be delivered to stroma, it is not clear how the non-invasive, pre-metastatic cancer cells overcome the diffusion barrier imposed by the dense ECM fibrils in the tumor microenvironment without MMP-facilitated ECM proteolysis. To investigate the possible mechanisms behind CAF induction, we constructed a 3D coculture system to mimic the *in vivo* microenvironment of early-stage breast cancer. The 3D coculture system allowed us to image the changes in ECM architectures, to measure the diffusion in ECM, and to track the cell motility in a dynamic and longitudinal manner. We observed that cancer cells align the ECM fibrils and induce CAF phenotypes in NFs. We also found that the fibril alignment is a force-dependent process mediated by RhoA signaling, and results in enhancing the diffusion of CAF-promoting exosomes secreted by cancer cells. By disrupting RhoA signaling or crosslinking ECM fibrils, ECM fibril alignment and diffusion enhancement is suppressed, and CAF induction reversed. We concluded that force generation and subsequent ECM remodeling play an important role during early-stage cancer development in CAF induction. Our finding may inspire a new cancer treatment strategy by optimally crosslinking the ECM fibrils, as demonstrated in this study, to suppress CAF induction and subsequent metastasis.

* Corresponding author. Department of Mechanical Engineering, Johns Hopkins University, Baltimore, MD, 21218, USA.)
E-mail address: yun.chen@jhu.edu (Y. Chen).

https://doi.org/10.1016/j.biomaterials.2020.119756
Received 19 September 2019; Received in revised form 28 December 2019; Accepted 2 January 2020
Available online 08 January 2020
0142-9612/

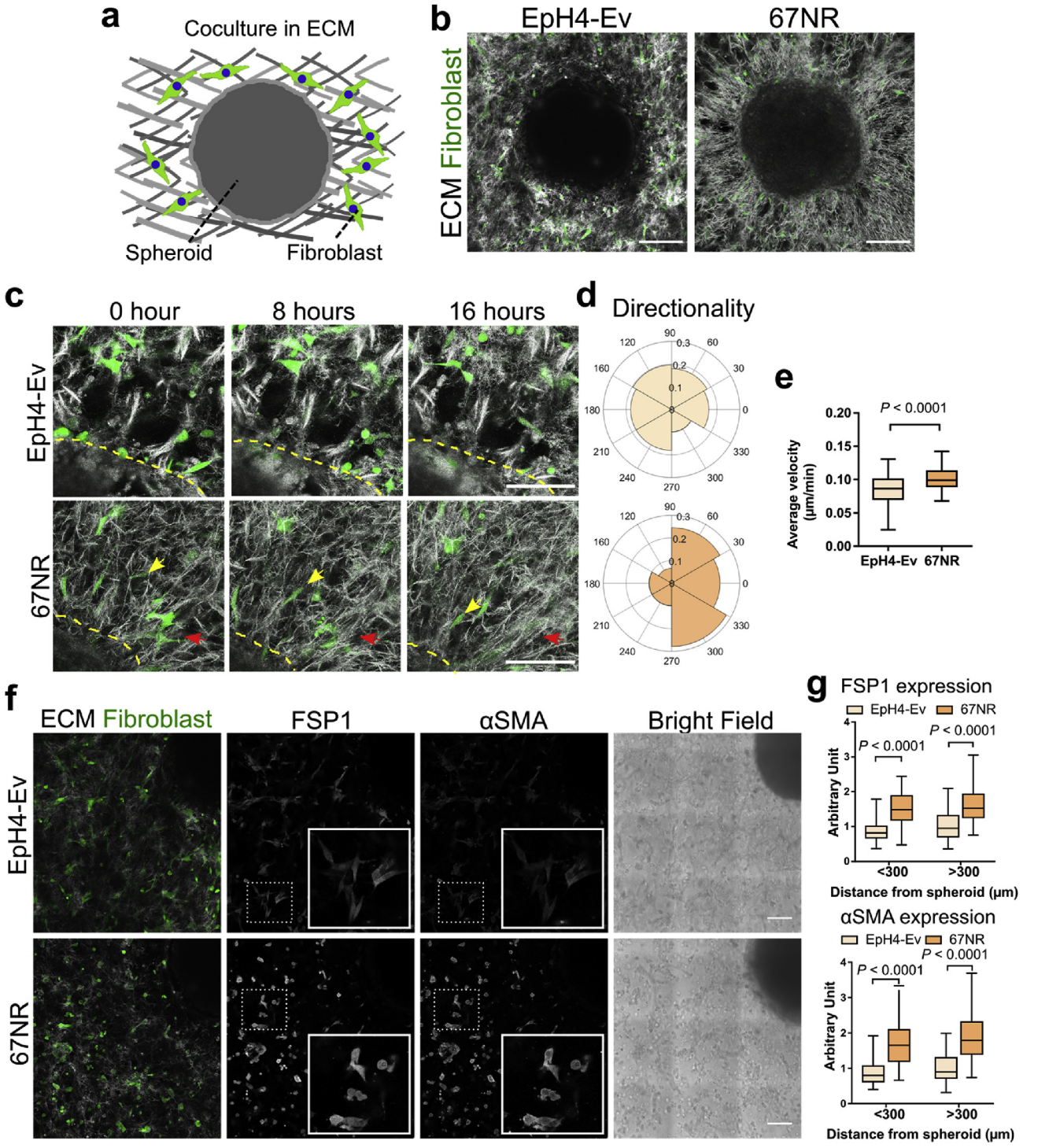

Fig. 1. | Coculturing early-stage breast cancer cells with fibroblasts causes ECM fibrils alignment and induces CAF-associated phenotypes. a, The schematic depicts the model system where a tumor spheroid embedded in ECM with fibroblasts in the periphery. **b**, ECM fibrils were radially aligned in the coculture of a 67NR spheroid and GFP-transfected fibroblasts (right), while the fibrils remained isotropic in the coculture containing EpH4-Ev and GFP-transfected fibroblasts (left). **c,** Fibroblasts (green) cocultured with an EpH4-Ev or 67NR spheroid migrated through the ECM over time. The dotted yellow lines trace the boundary of spheroids. The yellow arrows indicate the same fibroblast at different time points. The red arrows indicate local fibril alignment. **d**, Fibroblasts cocultured with 67NR spheroids (bottom) showed persistent migration toward the spheroid (right half of the rose chart), but not the ones cocultured with EpH4-Ev (top). EpH4-Ev: N = 61, 67NR: N = 61. **e**, Fibroblasts cocultured with 67NR spheroids showed higher velocity. EpH4-Ev: N = 72, 67NR: N = 61. **f**, **g**, CAF markers FSP1 and αSMA showed higher expression in fibroblasts cocultured with 67NR spheroids. The fibroblasts within and outside the 300-μm perimeter from the spheroid were analyzed separately. All data were normalized to the average from the EpH4-Ev > 300 μm EpH4-Ev: N = 81 (< 300 μm) and 83 (> 300 μm), 67NR: N = 83 (< 300 μm) and 76 (> 300 μm). Scale bars: (**b**) 200 μm, (**c**, **f**) 100 μm. (For interpretation of the references to colour in this figure legend, the reader is referred to the Web version of this article.)

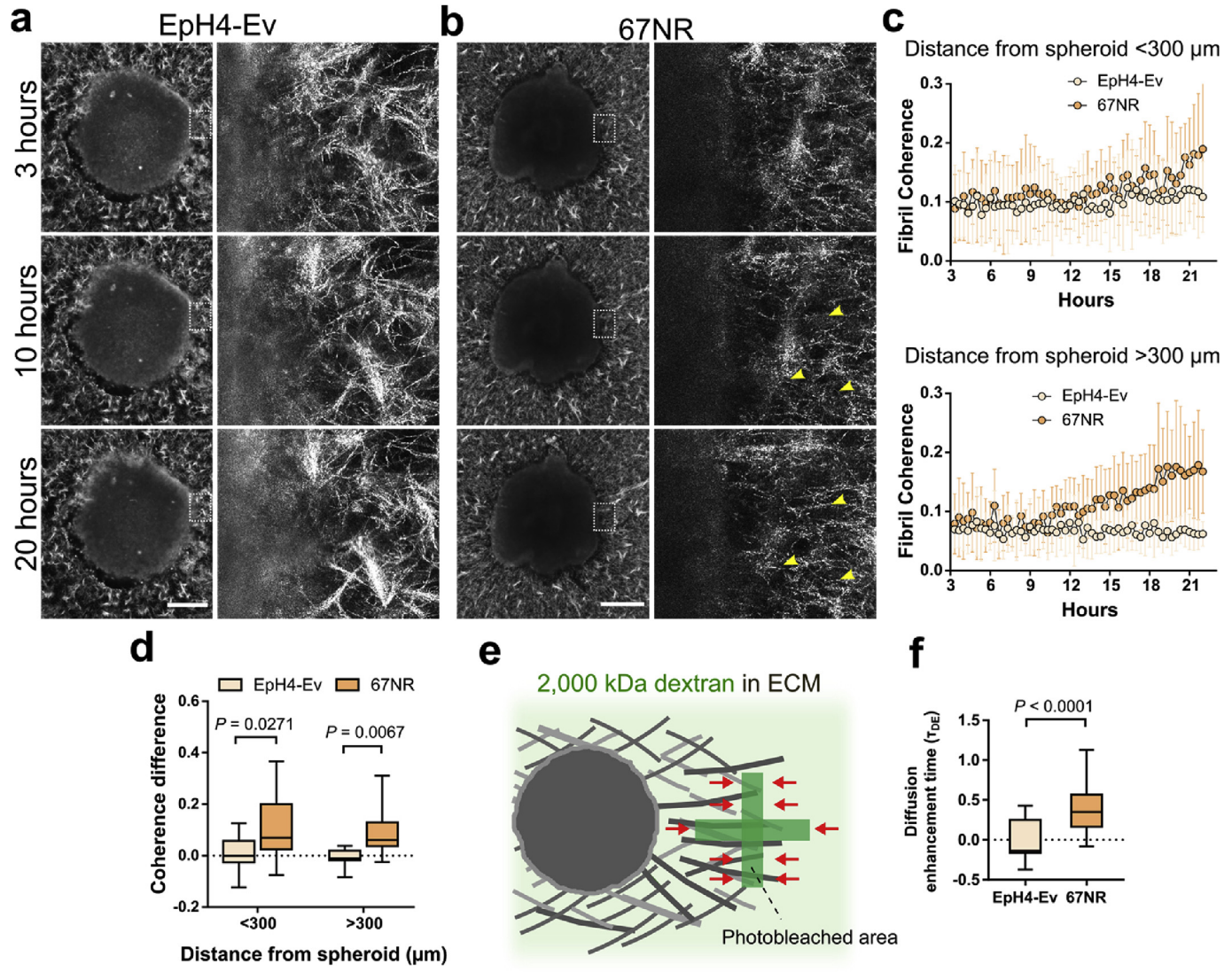

Fig. 2. | Early-stage cancer cells align the ECM fibrils and facilitate faster diffusion towards stroma. a, **b**, Time-lapse images showed that ECM fibrils were reoriented to be aligned over time in the 67NR spheroid-only, but not EpH4-Ev spheroid-only culture. Yellow arrowheads indicate the aligned fibrils. **c**, Fibril coherence analysis showed that in 67NR spheroid-only cultures, higher fibril alignment increased over time within and outside the 300-μm perimeter from the spheroid. **d**, The difference between fibril coherence at 3-h and 20-h incubation was quantified. ECM fibril alignment was increased by 67NR spheroids. For (**c**) and (**d**), EpH4-Ev: N = 12 (< 300 μm) and 10 (> 300 μm), 67NR: N = 13 (< 300 μm) and 10 (> 300 μm). **e**, Schematic of the line FRAP experiment depicts that 2000 kDa dextran-FITC is added to the spheroid-embedded ECM to be photobleached in the shape of two orthogonally oriented stripes: one along to the fibrils originated from the spheroid, the other perpendicular to the first stripe. The red arrows indicate the radial diffusion relative to the spheroid. If the diffusion in the radial direction is significantly faster, the recovery in the orthogonal stripe would be faster, because there is a shorter gap for the radially diffusing dextran-FITC to fill. **f**, Diffusion enhancement time τ_{DE} was increased by 67NR spheroids. EpH4-Ev: N = 25, 67NR: N = 34. Scale bar: (**a**) 200 μm. (For interpretation of the references to colour in this figure legend, the reader is referred to the Web version of this article.)

2. Results

2.1. The coculture of early-stage breast cancer cells and fibroblasts shows the ECM fibrils alignment and fibroblast activation

To examine the interaction between cancer cells and the fibroblasts in the stroma, spheroids consisting of mouse mammary epithelial cells EpH4-Ev, 67NR, or 4T1 were embedded in the 3D ECM, where fibroblasts NIH-3T3 were also present, mimetic of the distribution of these two cell types in the mammary gland (Fig. 1a). EpH4-Ev, 67NR and 4T1 cells were chosen because they respectively exhibit characteristics typical of normal, non-metastatic cancer and metastatic cancer cells from the same mouse strain (BALB/c), thereby isogenic [29,30]. The ratio between the numbers of epithelial cells and fibroblasts in the coculture are known to affect cell proliferation and gene expression [31–34]. Given that the *in vivo* ratio between epithelial cells and fibroblasts in the mammary gland during early stages of breast cancer ranges from 2:1 to 3: 1 (epithelial cells: fibroblasts) [34], we seeded cells accordingly after factoring in cell proliferation rates during the 2-day period when the spheroids were formed, to achieve the ratio of approximately 2.2 : 1 (epithelial cells: fibroblasts, Fig. S1). To distinguish between cell types in cocultures, fibroblasts were permanently transfected with green fluorescence protein (GFP). ECM fibrils were imaged using internal reflectance microscopy (IRM). After 24 hours of coculturing, ECM fibrils in 67NR-fibroblast cocultures were radially aligned, whereas fibrils in the EpH4-Ev-fibroblast coculture remained isotropically oriented (Fig. 1b and c, Video 1–5). Notably, fibroblasts cocultured with the 67NR spheroid showed directionally persistent migration toward the spheroid, whereas the fibroblasts with EpH4-Ev migrated without preferences (Fig. 1d). The average velocity of fibroblasts cocultured

with 67NR was 1.2-fold higher than the ones with EpH4-Ev (Fig. 1e). To examine whether cell migration pattern is associated with CAF induction [9,35], the cocultured fibroblasts were examined by immunofluorescence against widely used CAF markers FSP1 and αSMA [36,37]. The fibroblasts located within the 300-μm perimeter from the 67NR spheroid showed 1.8-fold higher FSP1 expression than the ones located within 300-μm perimeter from the EpH4-Ev spheroid (Fig. 1f). The fibroblasts located outside the 300-μm perimeter from the 67NR spheroid showed 1.6-fold higher FSP1 expression than the ones located outside the 300-μm perimeter from the EpH4-Ev spheroid (Fig. 1f). Similarly, the fibroblasts located within the 300-μm perimeter from the 67NR spheroid showed 2.0 -fold higher αSMA expression than the ones located within the 300-μm perimeter from the EpH4-Ev spheroid (Fig. 1g). The fibroblasts located outside the 300-μm perimeter from the 67NR spheroid showed 1.9-fold higher αSMA expression than the ones outside the 300-μm perimeter from the EpH4-Ev spheroid. CAF marker upregulation in fibroblasts separated from the 67NR spheroid by the distance of 300 μm or more suggests CAFs can be induced by long-range mechanisms. To confirm the validity of the immunofluorescence assay, the upregulated expression of FSP1 and αSMA in fibroblasts were also examined in Western blot using the same antibodies. The Western blot results agreed with the observation in immunofluorescence (Fig. S2).

Supplementary video related to this article can be found at https://doi.org/10.1016/j.biomaterials.2020.119756.

We observed that 4T1 spheroids rapidly disassembled (Fig. S3) and individual 4T1 cells migrated into the stroma, exhibiting the characteristic invasive behavior due to its high metastatic potential [38]. As 4T1 cells migrated into the stroma, they established direct contact with stromal fibroblasts. As a result of the invasion (Fig. S4), the initial exosome diffusion barrier between the 4T1 spheroid and stromal fibroblasts no longer existed. Therefore, in the following experiments designed to identify the mechanisms by which the exosome diffusion barrier is overcome, 4T1 cells were not used.

2.2. Early-stage breast cancer cells align the ECM fibrils and facilitate faster diffusion towards stroma

The observation that fibrils were radially aligned in the 67NR-fibroblast coculture, but not in the EpH4-Ev-fibroblast coculture, suggests 67NR is important for alignment. To determine whether the 67NR spheroid alone is sufficient to align the fibrils, time-lapse imaging was performed by embedding EpH4-Ev and 67NR spheroids in ECM without fibroblasts. After 24-h incubation, the EpH4-Ev spheroid-embedded fibrils remained isotropic (Fig. 2a, Video 6), whereas 67NR spheroid-embedded fibrils were aligned (Fig. 2b, Video 7). To quantify the degree of fibril alignment, coherence analysis [39] was performed. Higher coherence scores represent more alignment. Fibril orientations within and outside the 300-μm perimeter from the spheroid were evaluated separately. The score associated with EpH4-Ev spheroids remained unchanged, whereas the score associated with 67NR spheroids gradually increased (Fig. 2c and d). The coherence score increased by 0.1 from 3-h to 20-h incubation for fibrils incubated with 67NR, whereas the score with EpH4-Ev remained unchanged (Fig. 2d).

Supplementary video related to this article can be found at https://doi.org/10.1016/j.biomaterials.2020.119756.

We postulated that there is a causal relationship between the simultaneous observations of radially aligned fibrils in the 67NR-fibroblast coculture and higher CAF marker expression, possibly mediated by exosomes. Exosomes secreted by cancer cells can activate fibroblasts via TGF-β and miRNA contained within [40–42]. CAF phenotypes might be induced by exosomes secreted from the 67NR spheroid; and the fibril alignment favored efficient exosome transport in ECM. First, we verified whether exosomes secreted by 67NR are responsible for the increased expression of CAF markers in fibroblasts: we collected the medium from the 67NR culture and removed exosomes by ultracentrifugation [43]. Fibroblasts cultured in the exosome-depleted supernatant showed ~20% less FSP1 and αSMA expression than the ones cultured in the uncentrifuged medium (Fig. S5), suggesting the observed CAF marker upregulation in fibroblasts resulted from the exosomes secreted by 67NR.

Next, we examined whether the fibril alignment can affect exosome diffusion. We performed line fluorescence recovery after photobleaching (FRAP) [44] to measure the diffusivity in the spheroid-embedded ECM. The 2000-kDa FITC-conjugated dextran was used as the bleachable probe added to the ECM, because its molecular size is comparable to the exosomes secreted by 67NR [43]. Two orthogonally oriented stripes were selected as the region of interest for photobleaching: one in the radial direction to spheroid, the other perpendicular to the first stripe (Fig. 2e). To assess whether there is enhancement in diffusion rates in the radial direction from the spheroid, the metric "diffusion enhancement time (τ_{DE})" was introduced, defined as the difference in the characteristic fluorescence recovery times τ_D , when 64% of the fluorescence intensity is recovered, between the two stripes:

$$\tau_{DE} = \tau_{D(radial)} - \tau_{D(orthogonal)}$$

where $\tau_{D(radial)}$ represents the τ_D measured in the radial direction, and $\tau_{D(orthogonal)}$ in the corresponding orthogonal direction. If the diffusion rate is faster in the radial direction, $\tau_{D(orthogonal)}$ will be shorter, since the orthogonal stripe presents a smaller photobleached gap for the radially diffusing FITC-dextran to fill (Fig. 2e). Therefore, positive τ_{DE} values represent faster diffusion rates in the radial direction compared to the orthogonal direction. The τ_{DE} value in 67NR spheroid-embedded ECM was 0.4 s, and ~0 for EpH4-Ev-embedded ECM. Taken together, the results suggest radially aligned fibrils facilitate faster radial diffusion of exosomes (Fig. 2f).

2.3. Fibril alignment enhances exosome diffusion and CAF induction

To test whether the fibril alignment and the subsequent enhanced exosome diffusion induce CAF phenotypes, collagen mixed with 200-nm paramagnetic particles and fibroblasts was placed in a uniform magnetic field and allowed to polymerize. Upon polymerization, medium harvested from the 67NR culture was supplied through a reservoir (Fig. 3a). Visually, ECM fibrils polymerized in the magnetic field were aligned, whereas the control remained isotropic (Fig. 3b). The coherence score of fibrils subjected to the magnetic field was higher by 0.1 than the control (Fig. 3c). The line FRAP results correspondingly showed 2.1-fold higher τ_{DE} values in ECM subjected to magnetic field than the control (Fig. 3d). These results suggest that the magnet field effectively aligned fibrils and enhanced directional diffusion. Immunostaining was then performed to evaluate CAF induction. In the unaligned group, fibroblasts located more than 3000-μm away from the reservoir showed 39% and 47% lower FSP1 and αSMA expression, respectively, than the ones located within 1000-μm. In contrast, there was no difference between the two locations in the aligned group (Fig. 3e–g).

To visualize the effect of aligned ECM fibrils on the transport of exosomes or objects of the same size, 100-nm fluorescent particles were added to one of the reservoirs. The movements of the particles were then recorded in timelapse images (Figs. S6a and b, Video 8, 9). By tracking the displacement of the particles over time [45], it was observed that the particles moved fast (0.2935 μm/s) along the aligned ECM fibrils, whereas the particles moved much slower (0.0002 μm/s) if the ECM fibrils were not aligned. The observation at the single-particle level agrees with the results of the bulk measurement obtained in the FRAP experiments, leading us to deduce that fibril alignment enhances the anisotropic diffusion of exosomes and facilitates them to reach the fibroblasts further away from the cancer cells.

Supplementary video related to this article can be found at https://doi.org/10.1016/j.biomaterials.2020.119756.

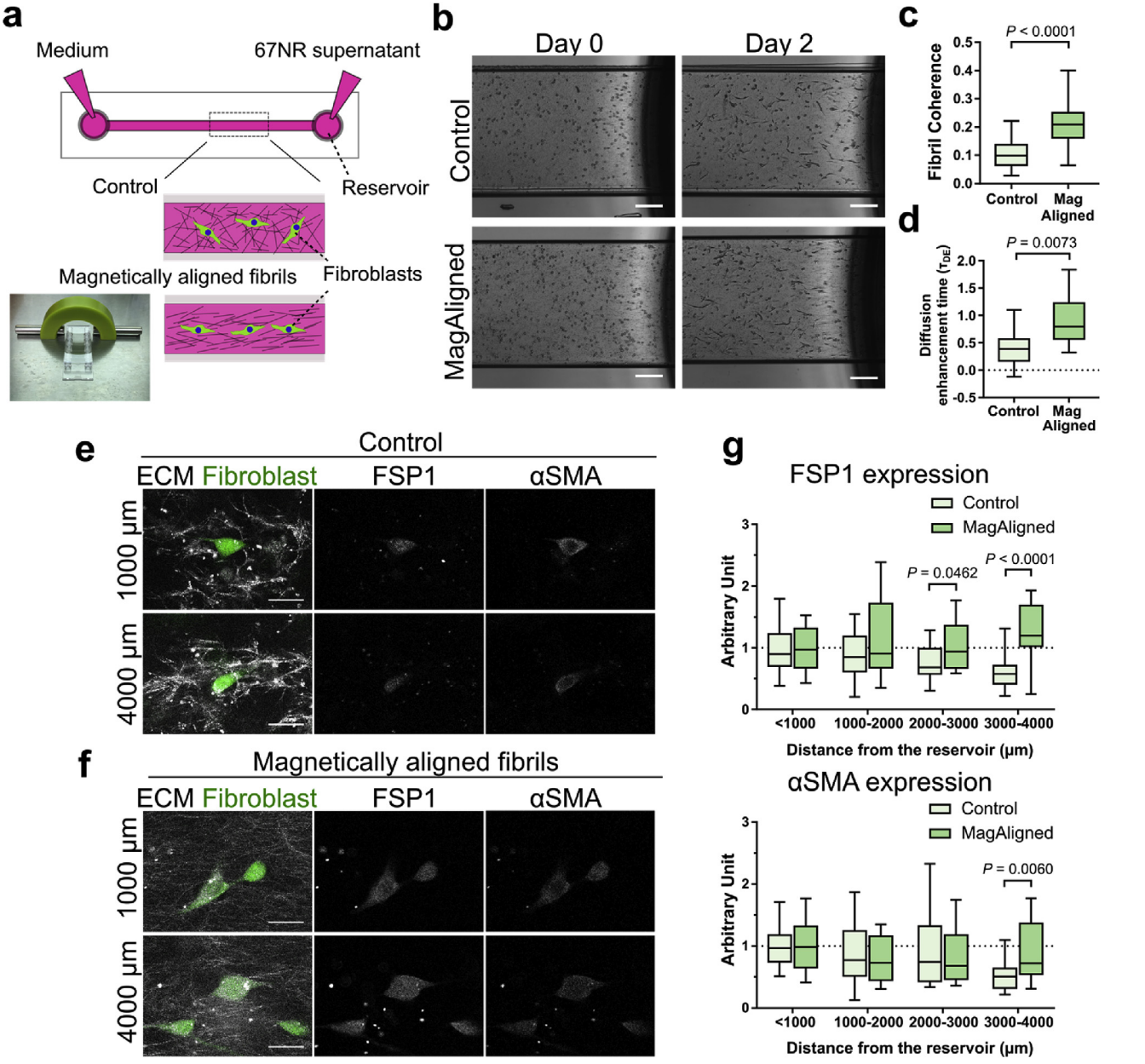

Fig. 3. | Fibrils alignment facilitates anisotropic diffusion of exosomes and increases CAF marker expression. a, The magnet pair (inset) was used to align ECM fibrils mixed with paramagnetic nanoparticles. Supernatant from 67NR-cultured medium and DMEM were added to the reservoirs. **b**, Fibroblasts were oriented correspondingly after being cultured in the magnetically aligned ECM for two days. **c**, Magnetically aligned ECM fibrils showed higher coherence scores. Control: N = 100. Aligned ECM: N = 93. **d**, Diffusion enhancement was observed in magnetically aligned fibrils in the aligned direction. Control: N = 10. Aligned ECM: N = 15. **e**, **f**, The FSP1 and αSMA expression was higher in fibroblasts grown in magnetically aligned ECM. **g**, The FSP1 and αSMA expression were quantified at various distances away from the 67NR-supernatant supplemented reservoir. All data were normalized to the average of the < 1000 μm group. For FSP1, control: N = 25 (< 1000 μm), 15 (1000–2000 μm), 21 (2000–3000 μm), and 21 (3000–4000 μm), aligned ECM: N = 27 (< 1000 μm), 13 (1000–2000 μm), 9 (2000–3000 μm), and 15 (3000–4000 μm). For αSMA, control: N = 25 (< 1000 μm), 15 (1000–2000 μm), 21 (2000–3000 μm), and 20 (3000–4000 μm), aligned ECM: N = 26 (< 1000 μm), 13 (1000–2000 μm), 9 (2000–3000 μm), and 12 (3000–4000 μm). Scale bars: (**b**) 200 μm, (**e**, **f**) 25 μm.

2.4. Prevention of ECM reorganization attenuates CAF induction

The corollary to our observation that ECM fibril alignment promotes CAF induction in the coculture is that suppressing such alignment will attenuate it. To confirm this, genipin, a biocompatible crosslinking reagent [46–48], was used to suppress the fibril reorganization. First, we identified the optimal genipin concentration to be 0.5 mM. 67NR-embedded ECM treated by 0.5 mM genipin for 24 h exhibited no observable cytotoxicity and negligible ECM stiffening (Fig. 4d). Yet the fibril alignment was suppressed by 28% (Fig. 4a and b). Correspondingly, the τ_{DE} value decreased to a negligible level (Fig. 4c). Though ECM crosslinking might lead to CAF induction because of ECM stiffening [49], it was not the case in our experiments. The rheological measurement results showed that the elastic modulus of the ECM treated with 0.5 mM genipin was 755 ± 163 Pa (mean ± s.d.), comparable to the un-crosslinked ECM, while ECM treated with 1 mM genipin became stiffer by 29% (Fig. 4d).

Having had established the optimal genipin concentration to suppress fibril alignment, we used it to evaluate whether CAF induction in cocultured fibroblasts would be attenuated. As expected, in genipin-treated cocultures, the FSP1 and αSMA expression in the fibroblasts was reduced by 23% and 33% respectively within the 300-μm perimeter

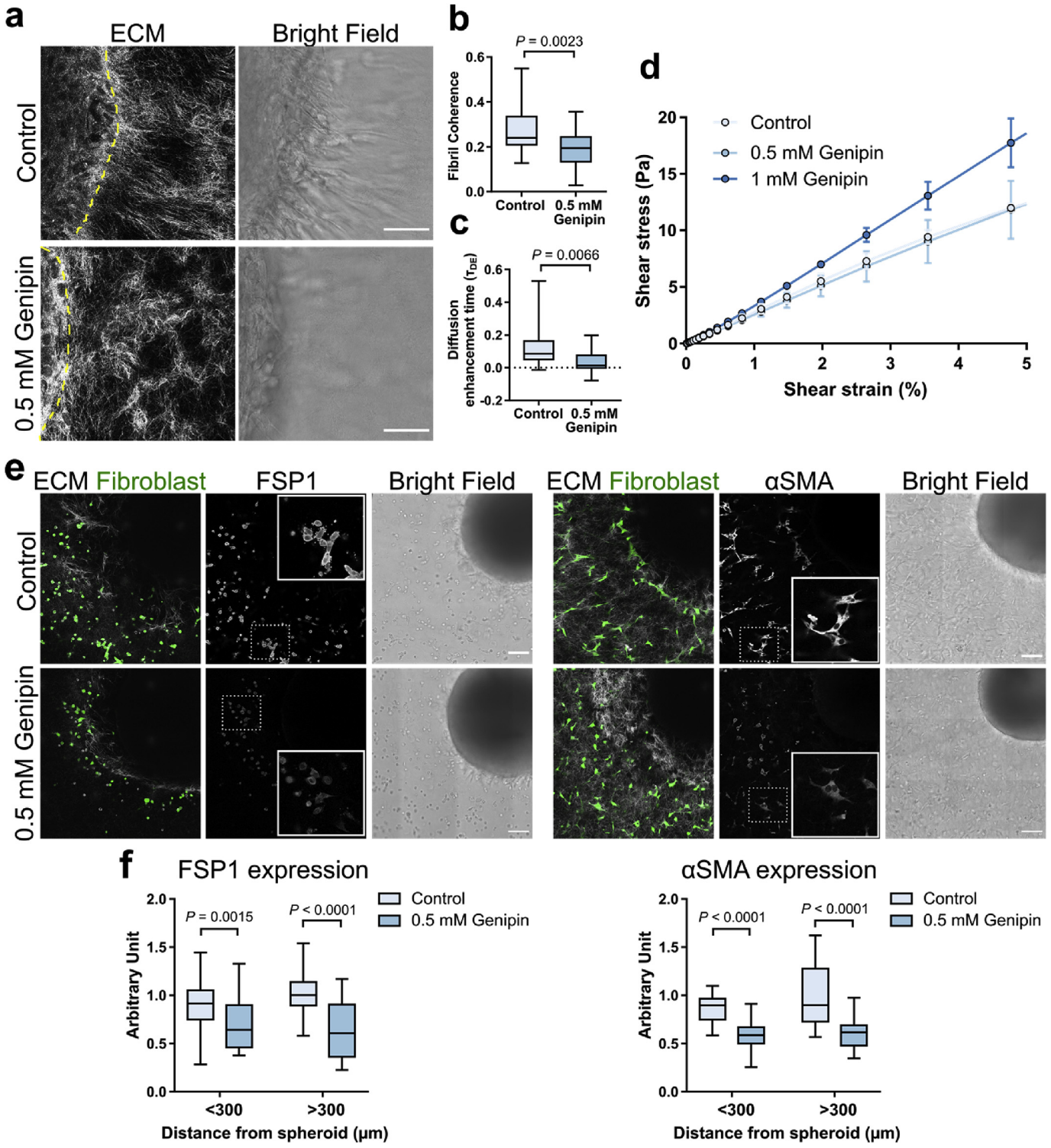

Fig. 4. | ECM crosslinking reduces fibril alignment and CAF induction. a, **b**, 67NR-embedded ECM treated with 0.5 mM genipin showed reduced alignment. Control: N = 20, 0.5 mM Genipin: N = 35. **c**, Diffusion enhancement was not observed in crosslinked ECM. Control: N = 25, 0.5 mM Genipin: N = 16. **d**, Rheological measurement showed that 0.5 mM genipin-treated ECM exhibits comparable shear moduli as the uncrosslinked control. Control: N = 3, 0.5 mM Genipin: N = 3, 1 mM Genipin: N = 2. **e**, **f**, The FSP1 and αSMA expression in fibroblasts from crosslinked cocultures was reduced. All data were normalized to the average from the control > 300 μm. For FSP1, control: N = 54 (< 300 μm) and 39 (> 300 μm), 0.5 mM Genipin: N = 20 (< 300 μm) and 16 (> 300 μm). For αSMA, control: N = 15 (< 300 μm) and 15 (> 300 μm), 0.5 mM Genipin: N = 45 (< 300 μm) and 45 (> 300 μm). Scale bars: (**a**) 50 μm, (**e**) 100 μm.

from the spheroid. The FSP1 and αSMA expression was further decreased by 36% and 39% respectively, when comparing fibroblasts located outside 300-μm perimeter between the treatment and the control (Fig. 4e and f). To exclude the possibility that genipin directly downregulates CAF markers in fibroblasts, we evaluated their expression in genipin-treated samples containing fibroblasts only (Figs. S7a, b, c). The FSP1 and αSMA expression remained unchanged in the fibroblast-only samples after genipin treatment, suggesting genipin reduces CAF marker expression in fibroblasts not in a direct manner, but through the suppression of ECM fibril alignment.

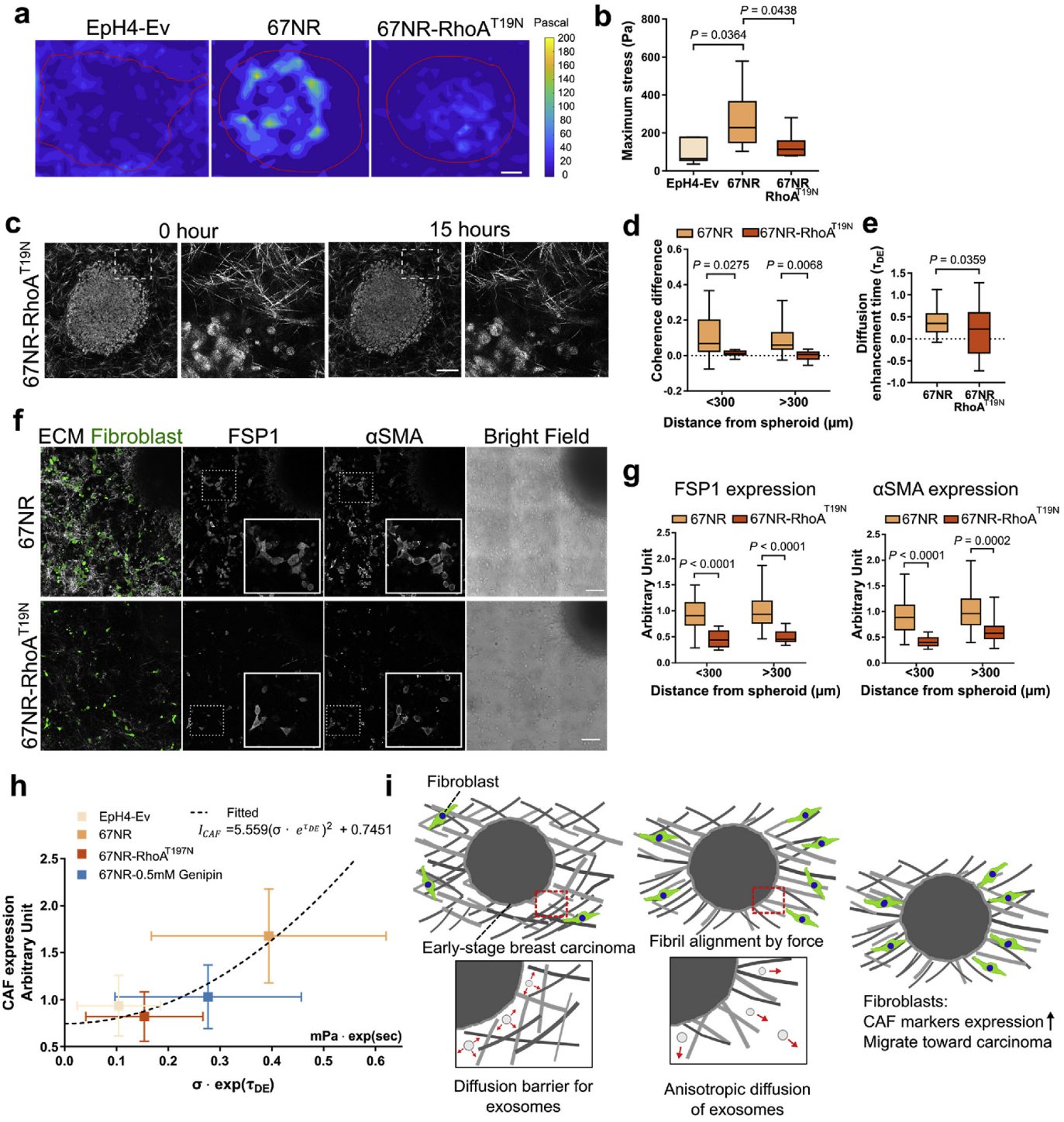

Fig. 5. | Fibril alignment and subsequent CAF induction by cancer cells is force-dependent. a, **b**, Traction force microscopy showed that expressing dominant negative RhoA, RhoA^{T19N}, reduced traction forces generated by 67NR spheroids. The shape of the spheroid is delineated by the red contour. EpH4-Ev: N = 7, 67NR: N = 6, 67NR-RhoA^{T19N}: N = 9. **c**, **d**, 67NR-RhoA^{T19N}-embedded ECM showed reduced fibril alignment. 67NR: N = 13 (< 300 μm) and 10 (> 300 μm), 67NR-RhoA^{T19N}: N = 11 (< 300 μm) and 11 (> 300 μm). **e**, 67NR-RhoA^{T19N}-embedded ECM showed no diffusion enhancement. 67NR: N = 34, 67NR-RhoA^{T19N}: N = 43. **f, g**, Fibroblasts cocultured with 67NR-RhoA^{T19N} spheroids showed reduced FSP1 and αSMA expression. All data were normalized to the average from the 67NR > 300 μm. For FSP1, 67NR: N = 83 (< 300 μm) and 76 (> 300 μm), 67NR-RhoA^{T19N}: N = 10 (< 300 μm) and 15 (> 300 μm). For αSMA, 67NR: N = 83 (< 300 μm) and 76 (> 300 μm), 67NR-RhoA^{T19N}: N = 9 (< 300 μm) and 15 (> 300 μm). **h, i**, The schematic illustrates our proposed model. Scale bars: (**a, c, f**) 100 μm. (For interpretation of the references to colour in this figure legend, the reader is referred to the Web version of this article.)

2.5. Fibril alignment and subsequent CAF induction by cancer cells is force-dependent

Reorientation of fibrils was prominent in the time-lapse images when 67NR spheroids were present (Video 1, 4, 5), implying that fibril alignment is a mechanical process and force-dependent. Relevantly, it was shown recently that, in the absence of MMP, cells in *C. elegans* deform ECM by mechanical forces during development [50]. To verify that 67NR spheroids align ECM fibril by mechanical forces, we performed 2D traction force microscopy to compare forces exerted by

67NR and EpH4-Ev spheroids. The spheroid-containing ECM was polymerized above a thin PDMS film decorated with fiducial fluorescent nanoparticles, so that forces generated by the spheroid displaced the nanoparticles, thereby informing force magnitudes generated by the spheroid. Adopting the assumption in previous studies [51] that force generation by spheroids is isotropic, and 2D results are proportional to 3D values, this measurement sufficed to compare the relative force generation capacity between 67NR and EpH4-Ev spheroids. 67NR spheroids generated 2.5-fold higher traction forces than EpH4-Ev (Fig. 5a and b). This higher force generation correlated with the more aligned ECM fibrils. To further prove the causality between forces, fibril alignment and CAF induction, 67NR cells expressing dominant negative form of RhoA (RhoA^{T19N}, Fig. S8) [52] were used in the coculture, so that RhoA-mediated force generation was inhibited [53,54]. The traction force microscopy results verified that 67NR-RhoA^{T19N} spheroids generated 51% less forces than their wildtype counterparts (Fig. 5a and b). 67NR-RhoA^{T19N} spheroids showed negligible radial alignment (Fig. 5c and d, Video 8). Furthermore, τ_{DE} in the 67NR-RhoA^{T19N} spheroid-embedded ECM was 59% less than τ_{DE} in the ECM with wildtype 67NR spheroids (Fig. 5e). Taken together, the results agree with the model where the early-stage breast cancer cells use high forces to align ECM fibrils and enhance exosome diffusion in the radial direction.

We next investigated whether suppressing force-dependent fibril alignment would reduce CAF induction in 67NR-RhoA^{T19N}-fibroblast cocultures. In terms of migration, we observed that the fibroblasts cocultured with 67NR-RhoA^{T19N} spheroids migrated without preferences (Figs. S9a and b, Video 9), with the average velocity 29% less than the ones with wildtype 67NR spheroids (Fig. S9c). The FSP1 and αSMA expression was attenuated by 51% and 54%, respectively, in fibroblasts within the 300-μm perimeter from the 67NR-RhoA^{T19N} spheroid; and decreased by 51% and 36%, for the ones outside the perimeter (Fig. 5f and g). To exclude the possibility that the decreased CAF induction directly resulted from impaired exosome secretion in 67NR-RhoA^{T19N} cells, we harvested media from 67NR-RhoA^{T19N} and wildtype 67NR cultures to incubate fibroblasts for 2 days. Fibroblasts incubated with media from 67NR-RhoA^{T19N} and wildtype 67NR cultures expressed αSMA and FSP1 at comparable levels, indicating the secretion of CAF-promoting factors is not impaired in 67NR-RhoA^{T19N} cells (Figs. S10a and b). Overall, the results demonstrate that force-dependent fibril alignment contributes to enhancing diffusion of CAF-promoting exosomes and subsequent CAF induction by early-stage breast cancer cells.

Additionally, high forces generated by cancer cells can potentially induce CAFs through other synergetic effects: it is plausible that as the ECM stiffens, resulting from force-dependent ECM fibril alignment [55], CAF phenotypes are reinforced in the fibroblasts [56]; high forces might further activate mechanosignaling pathways, also contributing to CAF induction [57–59]. Based on our data, the relation

$$I_{CAF} = \alpha\left(\sigma \cdot e^{\tau_{DE}}\right)^2 + I_{baseline}$$

could be used to gain insights to whether and to which extent forces contribute to CAF induction independent of enhanced diffusion (Fig. 5h), where I_{CAF} represents the index of CAF marker expression, σ is the maximum traction stress generated by the spheroid, τ_{DE} the diffusion enhancement time, $I_{baseline}$ is the baseline expression of CAF markers in non-CAF cells, and α is a coefficient which can be derived from curve fitting. In this study, α value was determined to be 0.7451 and $I_{baseline}$ was determined to be 0.4249.

3. Discussion

In this study, we illustrated that early-stage cancer cells can generate high forces to reorient ECM fibrils in the tumor microenvironment. Such reorientation results in radially aligned ECM fibrils where exosomes secreted by cancer cells diffuse more efficiently to reach stromal fibroblasts in the periphery. The CAF-promoting factors in the exosomes then upregulate genes manifesting CAF phenotypes in the fibroblasts (Fig. 5i). By either inhibiting force generation or directly suppressing ECM fibril alignment, CAF induction by cancer cells can be reversed. In summary, our study uncovers one of the mechanisms by which early-stage, pre-metastatic cancer cells induce CAFs to facilitate further tumor progression.

The finding in this study implies a potentially new strategy to suppress tumor progression clinically. For example, ECM crosslinking agents might be used to treat early-stage breast cancer, if an optimal concentration can be identified to both prevent the ECM fibril alignment, and avoid significant stiffening in ECM. Such strategy may be especially effective targeting the cancer cells exhibiting high actomyosin-based force generation, but low secretion of MMPs. Indeed, it was recently shown that supplementing the skin tissue with hyaluronan and proteoglycan link protein 1 (HAPLN1), which mediates the crosslinking of ECM fibrils, can prevent ECM fibrils from being aligned and subsequently suppress the progression of melanoma in aging mice [60]. Further *in vivo* studies and tests using tissues derived from patients are required to verify the feasibility of clinically applying crosslinking agents to treat cancer.

Although it has been shown that architecture of ECM fibrils can be modified by mechanical forces [9,61–64], our study is the first to link the change of diffusion patterns in ECM and the force-dependent ECM remodeling. From the general perspective of biomaterials, our finding implies the possibilities to control transports in biomaterials consisting of polymer chains by forces, including collagen, cytoskeleton monomers, alginate, fibronectin, cellulose, and synthetic biopolymers. The capacity of controlling the transport in biomaterials warrants the power of controlling cell fates by delivering nutrients, growth factors, cytokines, and drugs, on demands. The forces can be applied using magnetic forces [65], stretching [66], or shearing. Our finding presents a new tool, namely force-dependent control of molecular transports, to be added to the toolboxes of tissue engineers and synthetic biologists.

4. Materials and methods

Cell culture and transfection. EpH4-Ev and 4T1 cells were acquired from ATCC. 67NR cells were acquired from Karmanos Cancer Institute. GFP-transfected NIH-3T3 cells were acquired from Cell Biolabs. All the cell lines were cultured in Dulbecco's Modified Eagle Medium (DMEM) (Thermo Fisher) supplemented with 10% FBS (Thermo Fisher) and 1% penicillin-streptomycin (Thermo Fisher) at 37 °C in 5% CO_2. RhoA^{T19N} transfection was performed using lipofectamine 3000 (Thermo Fisher). RhoA^{T19N} plasmid was a gift from Dr. Gary Bokoch (Addgene plasmid # 12967; http://n2t.net/addgene:12967; RRID: Addgene_12967).

Coculture. Spheroid formation: the hanging drop method and hydrophobic wells were used sequentially to form spheroids [67]: Cells were resuspended in DMEM at the density of 5 × 10^4 cells per 40 μL and placed on the inner side of the lid of a cell culture dish. The droplets were placed at the interval of 300 mm. The dish was filled with 10 mL of PBS to provide humidity for the spheroids. The lid was then replaced back on to the dish. After incubation for 2 days, the spheroids were transferred to an ultra-low attachment 96-well plate (Corning, CLS7007) prefilled with 100 μL DMEM. The spheroids were then harvested for experiments within 4 days.

Spheroid placement: rat tail type I collagen (Corning, 354236) was diluted to 3 mg/mL by a mixture of 10x DMEM (Sigma-Aldrich, D2429) and 0.1 M NaOH at 3:1 ratio. Prior to embedding the spheroid, wells in a 24-well glass bottom dish (Cellvis, P24-0-N) were coated with 500 μL of 0.1% (w/v) Poly-L-Lysine solution (Sigma-Aldrich, P8920) for overnight at 4 °C. Upon the removal of Poly-L-Lysine solution, the wells were washed with 500 μL of PBS for 10 min, followed by air drying. 15 μL of collagen was added to the center of the well first and allowed to reach a partial gelling state at room temperature for 15 min. Then the spheroid

was transferred from the ultra-low attachment well to the center of the glass bottom well, where the spheroid was allowed to adhere to the gelling collagen for 30 min. The choices of collagen concentration (3 mg/mL) and the gelling temperature (room temperature) were made to achieve the stiffness of 755 ± 163 Pa (mean ± s.d., Fig. 4d) in the coculture, which is comparable to the stiffness of the mammary gland [68].

Spheroid encapsulation without fibroblast: after the spheroid adhered to the glass bottom well via collagen, the liquid collagen kept at the 4 ˚C was poured to the well to embed the spheroid. 40 μL liquid collagen was slowly pipetted into the well and allowed to gel for 2 h at room temperature. 2 mL DMEM was then added into the well. The embedded spheroid was incubated for at least 1 day or longer, as indicated in the text, before being used.

Spheroid encapsulation with fibroblasts: for coculture, 40 μL collagen was used to re-suspend 2×10^5 NIH-3T3 cells after centrifugation. The fibroblasts-containing liquid collagen was then added to the glass bottom well where a spheroid was placed in its center. The mixture was allowed to gel at room temperature for 2 h 2 mL DMEM was then added into the well. The embedded spheroid was incubated for at least 1 day or longer, as indicated in the text, before being used.

ECM alignment by an external magnetic field. The liquid collagen (3 mg/mL) was used to re-suspend fibroblasts to reach density of 10^6 cells/mL. The fibroblasts-containing collagen was then mixed with 200-nm magnetic particles (Chemicell, screenMAG/RR-Protein G, 2 mg/mL) in a ratio of 3:1.10 μL of the mixture was added to a flow chamber (Ibidi, μ-Slide VI 0.1) and treated with a pair of magnets positioned at both sides at room temperature for 10 min to align the fibrils [69]. For the control group, the mixture was placed at room temperature for 10 min without the magnets, followed by adding 50 μL medium in the both reservoirs of flow chamber and cultured in the incubator for 2 days. Afterwards, supernatant harvested from 67NR-culutred medium was added to one of the reservoirs, with the other filled with regular medium. Upon two days of culturing, cells in the flow channel were fixed with 4% paraformaldehyde for immunofluorescence.

ECM crosslinking. ECM-encapsulated 67NR spheroids were prepared as previously described. After 1-h incubation, genipin (Sigma-Aldrich, G4796) was mixed with DMEM to reach final concertation of 0.5 mM and 1 mM. The solutions were then added to the samples and incubated for 24 h. The DMSO-added DMEM were used as a control for the experiment. The samples were then washed with PBS for further usage.

Elastic modulus measurement. The Large Angle Oscillatory Shear (LAOS) was used to test the shear modulus of the crosslinked and uncrosslinked collagen gel. The collagen gel was prepared in disks and subjected to sinusoidal rotational deformation. The amplitude of the applied strain (γ) to the material was increased at a fixed rotational frequency (ω) of 1 rad/s. The analysis utilized a viscoelastic stress response model wherein the shear stress is computed as a function of strain ranging from 0.01%–15%. The Fourier Transform method is utilized to quantify the nonlinear stress response of ECM samples under increasingly large angular shear strain. LAOS was performed using an Anton Paar Modular Compact Rheometer (MCR 302) with a parallel plate (diameter 8 mm) at 37 ˚C. The measurement values of the shear modulus were then used obtain the elastic modulus by the formula:

$$E = 2G(1 + \nu)$$

where E is elastic modulus, G is shear modulus, and ν is the Poisson ratio. The Poisson ratio was assumed to be 0.5.

Immunofluorescence. Samples were fixed in 4% paraformaldehyde for 30 min, permeabilized with 0.1% Triton X-100 (Sigma-Aldrich, X100) in PBS for 30 min. PBS containing 2% bovine serum albumin (Sigma-Aldrich, A7906) and 0.1% Tween-20 (Promega) was then added to sample for 30 min for blocking. All antibody was diluted in PBS with 1% bovine serum albumin. The fixed cells were incubated with the primary antibody for overnight at 4 ˚C, followed by washing using PBS for 3 times, and then incubated with the secondary antibody for 2 h. After washing, the samples were immersed in PBS and stored in 4 ˚C for further usage. Dilution of antibodies used as follows: rabbit anti-FSP1 antibody (Millipore, S100A4, 1:500 dilution), mouse anti-αSMA antibody (Thermo Fisher, 1A4, 1:500 dilution), goat anti-rabbit IgG antibody conjugated with Alexa 647 (Jackson ImmunoResearch, 1:500 dilution), goat anti-mouse IgG antibody conjugated with DyLight 594 (abcam, 96873, 1:2000 dilution), goat anti-mouse IgG Antibody conjugated with Alexa 647 (BioLegend, 405322, 1:250 dilution). To avoid the strong autofluorescence emitted from crosslinked ECM [47] as the result of genipin reacting with amino acids [70] in the red channel, the immunostaining of the two CAF markers were performed separately in separate samples, both using the secondary antibody conjugated with Alexa 647.

Confocal microscopy. Imaging was performed using Leica TCS SP8 confocal microscope. Live cell imaging was performed with a 63× objective (NA 1.4) with pinhole set at one airy unit. An incubation chamber was used to maintain 37 ˚C, 5% CO_2, and humid air. Brightfield images were acquired in the transmitted light mode. 655-nm was used for IRM to visualize ECM fibrils. All the images of immunofluorescence were acquired by a 40× objective (NA 1.4) with pinhole was set at two airy units.

Western Blotting. NIH-3T3 cells were cultured in EpH4-Ev or 67NR supernatant for two days. Cells were then lysed using either RIPA buffer supplemented with protease and phosphatase inhibitors (Roche). Proteins were separated by 2% sodium dodecyl sulfate polyacrylamide gel electrophoresis (Mini-Protean TGX Gels, Bio-Rad), and transferred onto polyvinylidene difluoride membranes (Trans-Blot®, BioRad) using a semi-dry transfer apparatus (Bio-Rad). The membrane was incubated with the appropriate antibodies and ECL developing solution (GE). Dilution of antibodies used as follows: rabbit anti-FSP1 antibody (Millipore, S100A4, 1:1000 dilution), mouse anti-αSMA antibody (Thermo Fisher, 1A4, 1:1000 dilution), rabbit anti-GAPDH antibody (Sigma-Aldrich, G9545 1:1000), goat anti-rabbit IgG antibody conjugated with horseradish peroxidase (Jackson ImmunoResearch, 1:5000 dilution), goat anti-mouse IgG antibody conjugated with horseradish peroxidase (Jackson ImmunoResearch, 1:5000 dilution). GAPDH was used as a loading control.

Exosome depletion. To remove debris, medium harvested from the 67NR culture was first centrifuged at 1000 rpm for 10 min. The supernatant was transferred to a 4 mL ultracentrifuge tube (Beckman Ultra-Clear™) and centrifuged in a SW 60 Ti rotor (Beckman) at 40,000 rpm and 4 ˚C for 2 h [43]. The supernatant was then collected and used to culture fibroblasts. In addition, the harvested medium not subjected to ultracentrifugation was used as the control.

Traction force microscopy. The Silicone substrates (CY 52–276 A:B = 1:1) (Dow Corning) were prepared as previously described at room temperature [71]. The elastics modulus of the substrate was ~3 kPa. To conjugate microbeads fiduciary on the substrate, rhodamine carboxylate-modified microbeads (Thermo Fisher, F8801) were diluted from the tock in PBA at the ratio 1:25000. The bead solution was mixed with EDC (1-ethyl-3-(3- dimethylaminopropyl)) carbodiimide hydrochloride (Thermo Fisher, 22980) to achieve the final concentration of 200 μg/mL. The Silicone substrates were treated with 2% APTS ((3-Aminopropyl) triethoxysilane) (Sigma-Aldrich, 440140) diluted in PBS for 5 min at room temperature before the EDC-treated bead solution was added to the surface. The mixture was set to react for 4 h at room temperature. Afterwards, to minimize cytotoxicity, the substrates were immersed in PBS for 1 h at room temperature [72]. Before placing spheroids on the substrate, 200 μg/mL rat tail Type I Collagen was used to coat the surface for 1 h at 37 ˚C. Spheroids were then placed following the steps similar to the steps described above. Images documenting the positions of the fiduciary microbeads were first acquired with the spheroids adhered firmly to the substrate. The trypsinization (5%) was performed on-stage to detach the spheroid, followed by imaging the fiduciary microbeads again. The images before and after

trypsinization were then analyzed using the Traction Force Microscopy plugin for ImageJ [73].

Fluorescence recovery after photobleaching. 10 mg/mL of 2000 kDa fluorescein isothiocyanate (FITC)-Dextran (Sigma-Aldrich, FD2000S) was added to the collagen gel and incubated for 30 min at 37 °C. The dimensions used for photobleaching were 60 μm × 10 μm, 60 μm × 5 μm, and 20 μm × 2 μm for samples containing spheroids only, magnetically aligned ECM, and genipin-treated ECM, respectively. For the analysis, photobleaching was corrected using an exponential fit:

$$A \times e^{tB}$$

where t is the time point and A and B are fitting coefficients. Then on the bleaching corrected recovery curve, we employed a fitting equation of the following form:

$$a \times (1 - e^{-tb}) + c$$

where t is the time point and a, b and c are fitting coefficients to estimate the recovery time. The analysis was performed for both curves obtained through the radial and the orthogonal stripes. The characteristic fluorescence recovery times τ_D , when 64% of the fluorescence intensity is recovered, was calculated based on the fitted curve.

Tracking particles movement in aligned ECM. 20 μL of 100-nm diameter silver particles (Cytodiagnostics, S-100-20) (3.6×10^9 particles/mL) was added to one of the two reservoirs in the flow chamber containing either magnetically aligned collagen or unaligned control. The other reservoir was simultaneously filled 20 μL PBS. Timelapse images were acquired using IRM and bright-field microscopy. The displacement of the particles overtime and the velocity were evaluated using the Fiji plugin TrackMate [74] after applying the Laplacian mask to the raw images.

Imaging analysis. The cell velocity was measured using the free software CellTracker [75]. To measure the migration directionality, the line between the centroid of the cell and the centroid of line was first drawn, and the line linked the centroids of the same cell in the first and last frames was drawn. The angle between the two lines was then measured.

Fibril coherence analysis was performed using Quantitative orientation measurement in OrientationJ [39]. The immunostaining was quantified using Fiji/ImageJ software [76]. The noise from the background were subtracted by the following formula:

$$I = \frac{I_2 \times A_2 - I_1 \times A_1}{A_2 - A_1}$$

where the I_1 and A_1 denotes the fluorescence intensity, and the area of the cell, respectively. The I_2 and A_2 denotes the fluorescence intensity, and the area of the larger region encompassing the cell and the surrounding background, respectively. The larger region was traced by hand. The corrected fluorescence intensity was then recorded for each cell.

Statistical analysis. All the box and whisker plots shown in this work were produced by the software GraphPad Prism, where the box ranges from 25 to 75th percentile, with the middle line indicating the median, and the whisker indicating the minimum and maximum. For all the quantitative data, the error bars shown in the graphs represent standard errors; the P values were calculated by two-tailed unpaired Student's t-test.

Declaration of competing interest

The authors declare no competing or financial interests.

Acknowledgement

The authors thank Debonil Maity for technical assistance in analyzing the traction force microscopy data.

Appendix A. Supplementary data

Supplementary data to this article can be found online at https://doi.org/10.1016/j.biomaterials.2020.119756.

Author contributions

Y.C. conceived the study. W.-H.J., N.Y., and Y.C. designed the experiments. W.-H.J., N.Y., C.-C. C., K.E., and B. H. performed the experiments and data analysis. W.-H.J. and Y.C. wrote the manuscript.

References

[1] R. Navab, D. Strumpf, B. Bandarchi, C.-Q. Zhu, M. Pintilie, V.R. Ramnarine, E. Ibrahimov, N. Radulovich, L. Leung, M. Barczyk, D. Panchal, C. To, J.J. Yun, S. Der, F.A. Shepherd, I. Jurisica, M.-S. Tsao, Prognostic gene-expression signature of carcinoma-associated fibroblasts in non-small cell lung cancer, Proc. Natl. Acad. Sci. 108 (2011) 7160–7165, https://doi.org/10.1073/pnas.1014506108.

[2] Y. Takahashi, G. Ishii, T. Taira, S. Fujii, S. Yanagi, T. Hishida, J. Yoshida, M. Nishimura, H. Nomori, K. Nagai, A. Ochiai, Fibrous stroma is associated with poorer prognosis in lung squamous cell carcinoma patients, J. Thorac. Oncol. 6 (2011) 1460–1467, https://doi.org/10.1097/JTO.0b013e318229189d.

[3] J. Paulsson, P. Micke, Prognostic relevance of cancer-associated fibroblasts in human cancer, Semin. Cancer Biol. 25 (2014) 61–68, https://doi.org/10.1016/j.semcancer.2014.02.006.

[4] R.J. Buchsbaum, S.Y. Oh, Breast cancer-associated fibroblasts: where we are and where we need to go, Cancers (Basel) 8 (2016), https://doi.org/10.3390/cancers8020019.

[5] D. Öhlund, E. Elyada, D. Tuveson, Fibroblast heterogeneity in the cancer wound, J. Exp. Med. 211 (2014) 1503–1523, https://doi.org/10.1084/jem.20140692.

[6] C.S. Leung, T.L. Yeung, K.P. Yip, K.K. Wong, S.Y. Ho, L.S. Mangala, A.K. Sood, G. Lopez-Berestein, J. Sheng, S.T.C. Wong, M.J. Birrer, S.C. Mok, Cancer-associated fibroblasts regulate endothelial adhesion protein LPP to promote ovarian cancer chemoresistance, J. Clin. Investig. 128 (2018) 589–606, https://doi.org/10.1172/JCI95200.

[7] T. Liu, L. Zhou, D. Li, T. Andl, Y. Zhang, Cancer-associated fibroblasts build and secure the tumor microenvironment, Front. Cell Dev. Biol. 7 (2019) 60, https://doi.org/10.3389/fcell.2019.00060.

[8] E. Donnarumma, D. Fiore, M. Nappa, G. Roscigno, A. Adamo, M. Iaboni, V. Russo, A. Affinito, I. Puoti, C. Quintavalle, A. Rienzo, S. Piscuoglio, R. Thomas, G. Condorelli, Cancer-associated fibroblasts release exosomal microRNAs that dictate an aggressive phenotype in breast cancer, Oncotarget 8 (2017) 19592–19608, https://doi.org/10.18632/oncotarget.14752.

[9] B. Erdogan, M. Ao, L.M. White, A.L. Means, B.M. Brewer, L. Yang, M.K. Washington, C. Shi, O.E. Franco, A.M. Weaver, S.W. Hayward, D. Li, D.J. Webb, Cancer-associated fibroblasts promote directional cancer cell migration by aligning fibronectin, J. Cell Biol. 216 (2017) 3799–3816, https://doi.org/10.1083/jcb.201704053.

[10] K.O. Osuala, M. Sameni, S. Shah, N. Aggarwal, M.L. Simonait, O.E. Franco, Y. Hong, S.W. Hayward, F. Behbod, R.R. Mattingly, B.F. Sloane, Il-6 signaling between ductal carcinoma in situ cells and carcinoma-associated fibroblasts mediates tumor cell growth and migration, BMC Canc. 15 (2015) 584, https://doi.org/10.1186/s12885-015-1576-3.

[11] J.G. Goetz, S. Minguet, I. Navarro-Lérida, J.J. Lazcano, R. Samaniego, E. Calvo, M. Tello, T. Osteso-Ibáñez, T. Pellinen, A. Echarri, A. Cerezo, A.J.P. Klein-Szanto, R. Garcia, P.J. Keely, P. Sánchez-Mateos, E. Cukierman, M.A. Del Pozo, et al., Biomechanical remodeling of the microenvironment by stromal caveolin-1 favors tumor invasion and metastasis, Cell 146 (2011) 148–163, https://doi.org/10.1016/j.cell.2011.05.040.

[12] L. Tao, G. Huang, H. Song, Y. Chen, L. Chen, Cancer associated fibroblasts: an essential role in the tumor microenvironment, Oncol. Lett. 14 (2017) 2611–2620, https://doi.org/10.3892/ol.2017.6497.

[13] I. Jang, K.A. Beningo, Integrins, CAFs and mechanical forces in the progression of cancer, Cancers (Basel) 11 (2019), https://doi.org/10.3390/cancers11050721.

[14] F. Xing, J. Saidou, K. Watabe, Cancer associated fibroblasts (CAFs) in tumor microenvironment, Front. Biosci. 15 (2010) 166–179, https://doi.org/10.1080/00387010.2016.1211708.

[15] B. Apollonio, A.G. Ramsay, Exosomes and CAFs: partners in crime, Blood 126 (2015) 1053–1055, https://doi.org/10.1182/blood-2015-07-655233.

[16] Y. Attieh, A.G. Clark, C. Grass, S. Richon, M. Pocard, P. Mariani, N. Elkhatib, T. Betz, B. Gurchenkov, D.M. Vignjevic, Cancer-associated fibroblasts lead tumor invasion through integrin-β3-dependent fibronectin assembly, J. Cell Biol. 216 (2017) 3509–3520, https://doi.org/10.1083/jcb.201702033.

[17] A. Glentis, P. Oertle, P. Mariani, A. Chikina, F. El Marjou, Y. Attieh, F. Zaccarini, M. Lae, D. Loew, F. Dingli, P. Sirven, M. Schoumacher, B.G. Gurchenkov, M. Plodinec, D.M. Vignjevic, Cancer-associated fibroblasts induce metalloprotease-independent cancer cell invasion of the basement membrane, Nat. Commun. 8 (2017) 924, https://doi.org/10.1038/s41467-017-00985-8.

[18] A.E. Karnoub, A.B. Dash, A.P. Vo, A. Sullivan, M.W. Brooks, G.W. Bell, A.L. Richardson, K. Polyak, R. Tubo, R.A. Weinberg, Mesenchymal stem cells within tumour stroma promote breast cancer metastasis, Nature 449 (2007) 557–563, https://doi.org/10.1038/nature06188.

[19] L. Ying, Z. Zhu, Z. Xu, T. He, E. Li, Z. Guo, F. Liu, C. Jiang, Q. Wang, Cancer

associated fibroblast-derived hepatocyte growth factor inhibits the paclitaxel-induced apoptosis of lung cancer A549 cells by up-regulating the PI3K/Akt and GRP78 signaling on a microfluidic platform, PLoS One 10 (2015) e0129593, , https://doi.org/10.1371/journal.pone.0129593.
[20] N. Sato, N. Maehara, M. Goggins, Gene expression profiling of tumor-stromal interactions between pancreatic cancer cells and stromal fibroblasts, Cancer Res. 64 (2004) 6950–6956, https://doi.org/10.1158/0008-5472.CAN-04-0677.
[21] C.J. Olsen, J. Moreira, E.M. Lukanidin, N.S. Ambartsumian, Human mammary fibroblasts stimulate invasion of breast cancer cells in a three-dimensional culture and increase stroma development in mouse xenografts, BMC Canc. 10 (2010) 444, https://doi.org/10.1186/1471-2407-10-444.
[22] F.T. Borges, S.A. Melo, B.C. Özdemir, N. Kato, I. Revuelta, C. a Miller, V.H. Gattone, V.S. LeBleu, R. Kalluri, TGF-β1-containing exosomes from injured epithelial cells activate fibroblasts to initiate tissue regenerative responses and fibrosis, J. Am. Soc. Nephrol. 24 (2013) 385–392, https://doi.org/10.1681/ASN.2012101031.
[23] M. Chiba, M. Kimura, S. Asari, Exosomes secreted from human colorectal cancer cell lines contain mRNAs, microRNAs and natural antisense RNAs, that can transfer into the human hepatoma HepG2 and lung cancer A549 cell lines, Oncol. Rep. 28 (2012) 1551–1558, https://doi.org/10.3892/or.2012.1967.
[24] H. Valadi, K. Ekström, A. Bossios, M. Sjöstrand, J.J. Lee, J.O. Lötvall, Exosome-mediated transfer of mRNAs and microRNAs is a novel mechanism of genetic exchange between cells, Nat. Cell Biol. 9 (2007) 654–659, https://doi.org/10.1038/ncb1596.
[25] C. Théry, Exosomes: secreted vesicles and intercellular communications, F1000 Biol. Rep. 3 (2011) 15, https://doi.org/10.3410/B3-15.
[26] N. Erez, M. Truitt, P. Olson, D. Hanahan, Cancer-associated fibroblasts are activated in incipient neoplasia to orchestrate tumor-promoting inflammation in an NF-κB-Dependent manner, Cancer Cell 17 (2010) 135–147, https://doi.org/10.1016/j.ccr.2009.12.041.
[27] A. Rizki, V.M. Weaver, S.-Y. Lee, G.I. Rozenberg, K. Chin, C.A. Myers, J.L. Bascom, J.D. Mott, J.R. Semeiks, L.R. Grate, I.S. Mian, A.D. Borowsky, R.A. Jensen, M.O. Idowu, F. Chen, D.J. Chen, O.W. Petersen, J.W. Gray, M.J. Bissell, A human breast cell model of preinvasive to invasive transition, Cancer Res. 68 (2008) 1378–1387, https://doi.org/10.1158/0008-5472.CAN-07-2225.
[28] X.-J. Ma, S. Dahiya, E. Richardson, M. Erlander, D.C. Sgroi, Gene expression profiling of the tumor microenvironment during breast cancer progression, Breast Cancer Res. 11 (2009) R7 http://breast-cancer-research.biomedcentral.com/articles/10.1186/bcr2222 , Accessed date: 12 April 2016.
[29] A.M. Tester, N. Ruangpanit, R.L. Anderson, E.W. Thompson, MMP-9 secretion and MMP-2 activation distinguish invasive and metastatic sublines of a mouse mammary carcinoma system showing epithelial-mesenchymal transition traits, Clin. Exp. Metastasis 18 (2000) 553–560 http://www.ncbi.nlm.nih.gov/pubmed/11688960 , Accessed date: 23 May 2019.
[30] R. V Simões, I.S. Serganova, N. Kruchevsky, A. Leftin, A.A. Shestov, H.T. Thaler, G. Sukenick, J.W. Locasale, R.G. Blasberg, J.A. Koutcher, E. Ackerstaff, Metabolic plasticity of metastatic breast cancer cells: adaptation to changes in the microenvironment, Neoplasia 17 (2015) 671–684, https://doi.org/10.1016/j.neo.2015.08.005.
[31] M.F. Lefebvre, C. Guillot, M. Crepin, S. Saez, Influence of tumor derived fibroblasts and 1,25-dihydroxyvitamin D3 on growth of breast cancer cell lines, Breast Canc. Res. Treat. 33 (1995) 189–197, https://doi.org/10.1007/BF00665943.
[32] C. Gache, Y. Berthois, P.-M. Martin, S. Saez, Positive regulation of normal and tumoral mammary epithelial cell proliferation by fibroblasts in coculture, In Vitro Cell. Dev. Biol. Anim. 34 (1998) 347–351, https://doi.org/10.1007/s11626-998-0012-2.
[33] R.K. Chhetri, Z.F. Phillips, M.A. Troester, A.L. Oldenburg, Longitudinal study of mammary epithelial and fibroblast Co-cultures using optical coherence tomography reveals morphological hallmarks of pre-malignancy, PLoS One 7 (2012) e49148, , https://doi.org/10.1371/journal.pone.0049148.
[34] A. Sadlonova, Z. Novak, M.R. Johnson, D.B. Bowe, S.R. Gault, G.P. Page, J. V Thottassery, D.R. Welch, A.R. Frost, Breast fibroblasts modulate epithelial cell proliferation in three-dimensional in vitro co-culture, Breast Cancer Res. 7 (2004) R46, https://doi.org/10.1186/bcr949.
[35] E.T. Verghese, R. Drury, C.A. Green, D.L. Holliday, X. Lu, C. Nash, V. Speirs, J.L. Thorne, H.H. Thygesen, A. Zougman, M.A. Hull, A.M. Hanby, T.A. Hughes, MiR-26b is down-regulated in carcinoma-associated fibroblasts from ER-positive breast cancers leading to enhanced cell migration and invasion, J. Pathol. 231 (2013) 388–399, https://doi.org/10.1002/path.4248.
[36] A.-P. Sappino, O. Skalli, B. Jackson, W. Schürch, G. Gabbiani, Smooth-muscle differentiation in stromal cells of malignant and non-malignant breast tissues, Int. J. Cancer 41 (1988) 707–712, https://doi.org/10.1002/ijc.2910410512.
[37] P.J. Mishra, P.J. Mishra, R. Humeniuk, D.J. Medina, G. Alexe, J.P. Mesirov, S. Ganesan, J.W. Glod, D. Banerjee, Carcinoma-associated fibroblast-like differentiation of human mesenchymal stem cells, Cancer Res. 68 (2008) 4331–4339, https://doi.org/10.1158/0008-5472.CAN-08-0943.
[38] K. Tao, M. Fang, J. Alroy, G.G. Sahagian, Imagable 4T1 model for the study of late stage breast cancer, BMC Canc. 8 (2008) 228, https://doi.org/10.1186/1471-2407-8-228.
[39] E. Fonck, G.G. Feigl, J. Fasel, D. Sage, M. Unser, D.A. Rüfenacht, N. Stergiopulos, Effect of aging on elastin functionality in human cerebral arteries, Stroke 40 (2009) 2552–2556, https://doi.org/10.1161/STROKEAHA.108.528091.
[40] Q. Li, D. Zhang, Y. Wang, P. Sun, X. Hou, J. Larner, W. Xiong, J. Mi, MiR-21/Smad 7 signaling determines TGF-β1-induced CAF formation, Sci. Rep. 3 (2013) 2038, https://doi.org/10.1038/srep02038.
[41] C. Ringuette Goulet, G. Bernard, S. Tremblay, S. Chabaud, S. Bolduc, F. Pouliot, Exosomes induce fibroblast differentiation into cancer-associated fibroblasts through TGFβ signaling, Mol. Cancer Res. 16 (2018) 1196–1204, https://doi.org/10.1158/1541-7786.MCR-17-0784.
[42] T. Fang, H. Lv, G. Lv, T. Li, C. Wang, Q. Han, L. Yu, B. Su, L. Guo, S. Huang, D. Cao, L. Tang, S. Tang, M. Wu, W. Yang, H. Wang, Tumor-derived exosomal miR-1247-3p induces cancer-associated fibroblast activation to foster lung metastasis of liver cancer, Nat. Commun. 9 (2018) 191, https://doi.org/10.1038/s41467-017-02583-0.
[43] I. Vardaki, S. Ceder, D. Rutishauser, G. Baltatzis, T. Foukakis, T. Panaretakis, Periostin is identified as a putative metastatic marker in breast cancer-derived exosomes, Oncotarget 7 (2016) 74966–74978, https://doi.org/10.18632/oncotarget.11663.
[44] T. Stylianopoulos, B. Diop-Frimpong, L.L. Munn, R.K. Jain, Diffusion anisotropy in collagen gels and tumors: the effect of fiber network orientation, Biophys. J. 99 (2010) 3119–3128, https://doi.org/10.1016/j.bpj.2010.08.065.
[45] Y. Chen, B.C. Lagerholm, B. Yang, K. Jacobson, Methods to measure the lateral diffusion of membrane lipids and proteins, Methods 39 (2006) 147–153, https://doi.org/10.1016/j.ymeth.2006.05.008.
[46] A. Bigi, G. Cojazzi, S. Panzavolta, N. Roveri, K. Rubini, Stabilization of gelatin films by crosslinking with genipin, Biomaterials 23 (2002) 4827–4832, https://doi.org/10.1016/S0142-9612(02)00235-1.
[47] H.G. Sundararaghavan, G.A. Monteiro, N.A. Lapin, Y.J. Chabal, J.R. Miksan, D.I. Shreiber, Genipin-induced changes in collagen gels: correlation of mechanical properties to fluorescence, J. Biomed. Mater. Res. A 87A (2008) 308–320, https://doi.org/10.1002/jbm.a.31715.
[48] X. Zhang, X. Chen, T. Yang, N. Zhang, L. Dong, S. Ma, X. Liu, M. Zhou, B. Li, The effects of different crossing-linking conditions of genipin on type I collagen scaffolds: an in vitro evaluation, Cell Tissue Bank. 15 (2014) 531–541, https://doi.org/10.1007/s10561-014-9423-3.
[49] P.J. Wipff, D.B. Rifkin, J.J. Meister, B. Hinz, Myofibroblast contraction activates latent TGF-β1 from the extracellular matrix, J. Cell Biol. 179 (2007) 1311–1323, https://doi.org/10.1083/jcb.200704042.
[50] L.C. Kelley, Q. Chi, R. Cáceres, E. Hastie, A.J. Schindler, Y. Jiang, D.Q. Matus, J. Plastino, D.R. Sherwood, Adaptive F-actin polymerization and localized ATP production drive basement membrane invasion in the absence of MMPs, Dev. Cell 48 (2019) 313–328, https://doi.org/10.1016/j.devcel.2018.12.018 e8.
[51] M.P. Iwanicki, R.A. Davidowitz, M.R. Ng, A. Besser, T. Muranen, M. Merritt, G. Danuser, T. Ince, J.S. Brugge, Ovarian cancer spheroids use myosin-generated force to clear the mesothelium, Cancer Discov. 1 (2011) 144–157, https://doi.org/10.1158/2159-8274.CD-11-0010.
[52] M.C. Subauste, M. Von Herrath, V. Benard, C.E. Chamberlain, T.-H. Chuang, K. Chu, G.M. Bokoch, K.M. Hahn, Rho family proteins modulate rapid apoptosis induced by cytotoxic T lymphocytes and fas, J. Biol. Chem. 275 (2000) 9725–9733, https://doi.org/10.1074/jbc.275.13.9725.
[53] K.A. Beningo, K. Hamao, M. Dembo, Y.-L. Wang, H. Hosoya, Traction forces of fibroblasts are regulated by the Rho-dependent kinase but not by the myosin light chain kinase, Arch. Biochem. Biophys. 456 (2006) 224–231, https://doi.org/10.1016/j.abb.2006.09.025.
[54] Y.-T. Shiu, S. Li, W.A. Marganski, S. Usami, M.A. Schwartz, Y.-L. Wang, M. Dembo, S. Chien, Rho mediates the shear-enhancement of endothelial cell migration and traction force generation, Biophys. J. 86 (2004) 2558–2565, https://doi.org/10.1016/S0006-3495(04)74311-8.
[55] K.M. Riching, B.L. Cox, M.R. Salick, C. Pehlke, A.S. Riching, S.M. Ponik, B.R. Bass, W.C. Crone, Y. Jiang, A.M. Weaver, K.W. Eliceiri, P.J. Keely, 3D collagen alignment limits protrusions to enhance breast cancer cell persistence, Biophys. J. 107 (2014) 2546–2558, https://doi.org/10.1016/j.bpj.2014.10.035.
[56] F. Calvo, N. Ege, A. Grande-Garcia, S. Hooper, R.P. Jenkins, S.I. Chaudhry, K. Harrington, P. Williamson, E. Moeendarbary, G. Charras, E. Sahai, Mechanotransduction and YAP-dependent matrix remodelling is required for the generation and maintenance of cancer-associated fibroblasts, Nat. Cell Biol. 15 (2013) 637–646, https://doi.org/10.1038/ncb2756.
[57] F.J. Sulzmaier, C. Jean, D.D. Schlaepfer, FAK in cancer: mechanistic findings and clinical applications, Nat. Rev. Cancer 14 (2014) 598–610, https://doi.org/10.1038/nrc3792.
[58] R. Kalluri, M. Zeisberg, Fibroblasts in cancer, Nat. Rev. Cancer 6 (2006) 392–401, https://doi.org/10.1038/nrc1877.
[59] P. Gascard, T.D. Tlsty, Carcinoma-associated fibroblasts: orchestrating the composition of malignancy, Genes Dev. 30 (2016) 1002–1019, https://doi.org/10.1101/gad.279737.116.
[60] A. Kaur, B.L. Ecker, S.M. Douglass, C.H. Kugel, M.R. Webster, F.V. Almeida, R. Somasundaram, J. Hayden, E. Ban, H. Ahmadzadeh, J. Franco-Barraza, N. Shah, I.A. Mellis, F. Keeney, A. Kossenkov, H.-Y. Tang, X. Yin, Q. Liu, X. Xu, M. Fane, P. Brafford, M. Herlyn, D.W. Speicher, J.A. Wargo, M.T. Tetzlaff, L.E. Haydu, A. Raj, V. Shenoy, E. Cukierman, A.T. Weeraratna, Remodeling of the collagen matrix in aging skin promotes melanoma metastasis and affects immune cell motility, Cancer Discov. 9 (2019) 64–81, https://doi.org/10.1158/2159-8290.CD-18-0193.
[61] N. Saeidi, E.A. Sander, R. Zareian, J.W. Ruberti, Production of highly aligned collagen lamellae by combining shear force and thin film confinement, Acta Biomater. 7 (2011) 2437–2447, https://doi.org/10.1016/j.actbio.2011.02.038.
[62] B. Lanfer, U. Freudenberg, R. Zimmermann, D. Stamov, V. Körber, C. Werner, Aligned fibrillar collagen matrices obtained by shear flow deposition, Biomaterials 29 (2008) 3888–3895, https://doi.org/10.1016/j.biomaterials.2008.06.016.
[63] H. Wang, A.S. Abhilash, C.S. Chen, R.G. Wells, V.B. Shenoy, Long-range force transmission in fibrous matrices enabled by tension-driven alignment of fibers, Biophys. J. 107 (2014) 2592–2603, https://doi.org/10.1016/j.bpj.2014.09.044.
[64] P.V. Taufalele, J.A. VanderBurgh, A. Muñoz, M.R. Zanotelli, C.A. Reinhart-King, Fiber alignment drives changes in architectural and mechanical features in collagen

matrices, PLoS One 14 (2019) e0216537, , https://doi.org/10.1371/journal.pone.0216537.
[65] Y. Chen, S. Guzik, J.P. Sumner, J. Moreland, A.P. Koretsky, Magnetic manipulation of actin orientation, polymerization, and gliding on myosin using superparamagnetic iron oxide particles, Nanotechnology 22 (2011) 065101, , https://doi.org/10.1088/0957-4484/22/6/065101.
[66] Y. Chen, A.M. Pasapera, A.P. Koretsky, C.M. Waterman, Orientation-specific responses to sustained uniaxial stretching in focal adhesion growth and turnover, Proc. Natl. Acad. Sci. 110 (2013) E2352–E2361, https://doi.org/10.1073/pnas.1221637110.
[67] J.M. Kelm, N.E. Timmins, C.J. Brown, M. Fussenegger, L.K. Nielsen, Method for generation of homogeneous multicellular tumor spheroids applicable to a wide variety of cell types, Biotechnol. Bioeng. 83 (2003) 173–180, https://doi.org/10.1002/bit.10655.
[68] D.T. Butcher, T. Alliston, V.M. Weaver, A tense situation: forcing tumour progression, Nat. Rev. Cancer 9 (2009) 108–122, https://doi.org/10.1038/nrc2544.
[69] P.V. Taufalele, J.A. VanderBurgh, A. Muñoz, M.R. Zanotelli, C.A. Reinhart-King, Fiber alignment drives changes in architectural and mechanical features in collagen matrices, PLoS One 14 (2019) e0216537, , https://doi.org/10.1371/journal.pone.0216537.
[70] C. Djerassi, J.D. Gray, F.A. Kincl, Naturally occurring oxygen heterocyclics. IX.1 isolation and characterization of Genipin2, J. Org. Chem. 25 (1960) 2174–2177, https://doi.org/10.1021/jo01082a022.
[71] R.W. Style, R. Boltyanskiy, G.K. German, C. Hyland, C.W. Macminn, A.F. Mertz, L.A. Wilen, Y. Xu, E.R. Dufresne, Traction Force Microscopy in Physics and Biology, The Royal Society of Chemistry, 2014, https://doi.org/10.1039/c4sm00264d.
[72] E. Gutierrez, E. Tkachenko, A. Besser, P. Sundd, K. Ley, G. Danuser, M.H. Ginsberg, A. Groisman, High refractive index silicone gels for simultaneous total internal reflection fluorescence and traction force microscopy of adherent cells, PLoS One 6 (2011) e23807, , https://doi.org/10.1371/journal.pone.0023807.
[73] Q. Tseng, E. Duchemin-Pelletier, A. Deshiere, M. Balland, H. Guillou, O. Filhol, M. Thery, Spatial organization of the extracellular matrix regulates cell-cell junction positioning, Proc. Natl. Acad. Sci. 109 (2012) 1506–1511, https://doi.org/10.1073/pnas.1106377109.
[74] J.Y. Tinevez, N. Perry, J. Schindelin, G.M. Hoopes, G.D. Reynolds, E. Laplantine, S.Y. Bednarek, S.L. Shorte, K.W. Eliceiri, TrackMate: an open and extensible platform for single-particle tracking, Methods 115 (2017) 80–90, https://doi.org/10.1016/j.ymeth.2016.09.016.
[75] F. Piccinini, A. Kiss, P. Horvath, CellTracker (not only) for dummies, Bioinformatics 32 (2016) 955–957, https://doi.org/10.1093/bioinformatics/btv686.
[76] J. Schindelin, I. Arganda-Carreras, E. Frise, V. Kaynig, M. Longair, T. Pietzsch, S. Preibisch, C. Rueden, S. Saalfeld, B. Schmid, J.-Y. Tinevez, D.J. White, V. Hartenstein, K. Eliceiri, P. Tomancak, A. Cardona, Fiji: an open-source platform for biological-image analysis, Nat. Methods 9 (2012) 676–682, https://doi.org/10.1038/nmeth.2019.